APPLICATION OF ELECTRON-BEAM CONTROLLED DIFFUSE DISCHARGES TO FAST SWITCHING[+]

R.J. Commisso[a], R.F. Fernsler[a], V.E. Scherrer, and I.M. Vitkovitsky

Naval Research Laboratory
Washington, DC 20375

Summary

Recent investigations into the phenomena associated with electron-beam controlled diffuse discharges indicate a potential application for repetitive ($\geq$ 10 kHz, in a "burst" mode), high power ($\sim10^{10}$ W) switching. In such discharges the conductivity of the gas is regulated by the competition between beam ionization and attachment and recombination processes in the gas. Short opening times, limited in practice to the decay time of the electron beam, can be realized while high voltage is being applied to the switch. We report on one series of experiments using a N_2-O_2 combination in which the time dependence of the discharge current at two pressures has been determined. The results are compared to a zero-dimensional numerical simulation where the gas chemistry is coupled to the discharge circuit. Experiments exploring the advantages of gases with different collision cross sections and the behavior of the overall discharge stability have also been performed. A formalism for switch design in which the switch gas mixture and pressure, switch area and length are estimated self-consistently for a given system efficiency is reviewed. The formalism is used to design a single pulse, 200 kV, 30 kA (6 Ω), 100 ns FWHM inductive storage generator.

Introduction

The successful implementation of inductive energy storage and its inherent benefits to pulse power applications[1,2] depends critically on the development of opening switches. These switches must be capable of conducting current during the charging period of an inductor and then become sufficently resistive to divert the current flowing in the inductor to a load. The current commutation must occur on a time scale which is short compared to the inductor charging time and in the presence of an electric field across the switch that increases during the commutation process. Some applications require the switch to be capable of repetitively pulsed operation (see, for example, Ref. 3). Such a repetitively pulsed opening switch automatically satisfies the conditions required for operation as a repetitively pulsed closing switch.

Several authors[4-7] have reported on experiments and theoretical investigations in which an electron beam (e-beam) is used as an ionizing agent to sustain a diffuse (volumetric) discharge in a gas placed between two electrodes. The concept, as it might be used in a switching application, is illustrated in Fig. 1. In this scheme the gas resistivity at any time is determined by a competition between ionization provided by the beam and the various recombination and attaching processes characteristic of the specific gas mixture, pressure, and applied electric field. This, along with the volume discharge property, allows the gas to return to its original non-conducting state very quickly

once the source of ionization is removed. An arc discharge is avoided by proper switch design.[8] The switch length, pressure and area are maintained in such a way that self-sparking is avoided.
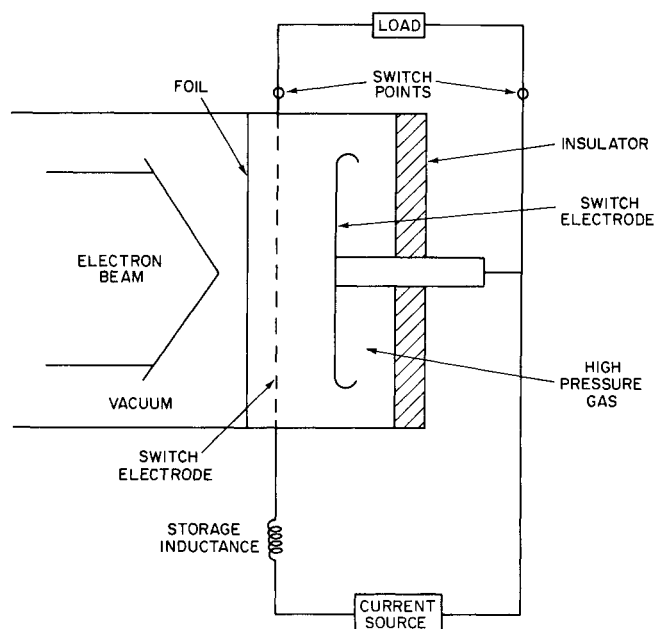

Fig. 1.   Illustration of opening switch application for an e-beam controlled diffuse discharge.

In this paper we present some theoretical analyses and data from an e-beam controlled diffuse discharge experiment that are relevant to understanding the physics associated with the behavior and optimization of an e-beam controlled switch (EBCS). Included in this are general equilibrium scaling laws, the consequence of using gases which exhibit unusual collision cross section behavior, and stability of the discharge. Because of the reliability and accessibility of various cross section data, most of the experiments were performed with mixtures of O_2 and N_2. Also reviewed is a design formalism[8] that self-consistently estimates the switch gas mixture, pressure, area, length and e-beam generator characteristics for a given system energy transfer efficiency, output pulse and number of pulses. Using this formalism we outline a design for an inductive storage system capable of delivering a single $\sim$ 200 kV, $\sim$ 100 ns full width at half maximum (FWHM), $\sim$ 30 kA pulse into a $\sim$ 6 Ω load.

Description of Experiment

A schematic of the experimental apparatus is shown in Fig. 2. An inductively driven e-beam diode system, in which two exploding wire fuses are used in sequence as opening switches to

Report Documentation Page

1. REPORT DATE **JUN 1983**	2. REPORT TYPE **N/A**	3. DATES COVERED **-**
4. TITLE AND SUBTITLE **Application Of Electron-Beam Controlled Diffuse Discharges To Fast Switching**		5a. CONTRACT NUMBER
		5b. GRANT NUMBER
		5c. PROGRAM ELEMENT NUMBER
6. AUTHOR(S)		5d. PROJECT NUMBER
		5e. TASK NUMBER
		5f. WORK UNIT NUMBER
7. PERFORMING ORGANIZATION NAME(S) AND ADDRESS(ES) **Naval Research Laboratory Washington, DC 20375**		8. PERFORMING ORGANIZATION REPORT NUMBER
9. SPONSORING/MONITORING AGENCY NAME(S) AND ADDRESS(ES)		10. SPONSOR/MONITOR'S ACRONYM(S)
		11. SPONSOR/MONITOR'S REPORT NUMBER(S)

12. DISTRIBUTION/AVAILABILITY STATEMENT
Approved for public release, distribution unlimited

13. SUPPLEMENTARY NOTES
See also ADM002371. 2013 IEEE Pulsed Power Conference, Digest of Technical Papers 1976-2013, and Abstracts of the 2013 IEEE International Conference on Plasma Science. Held in San Francisco, CA on 16-21 June 2013. U.S. Government or Federal Purpose Rights License

14. ABSTRACT

15. SUBJECT TERMS

16. SECURITY CLASSIFICATION OF:			17. LIMITATION OF ABSTRACT	18. NUMBER OF PAGES	19a. NAME OF RESPONSIBLE PERSON
a. REPORT **unclassified**	b. ABSTRACT **unclassified**	c. THIS PAGE **unclassified**	**SAR**	**7**	

produce a high voltage pulse across the diode, provides the e-beam for the switch experiments. This system has been described in detail elsewhere.[9] Generation of a second e-beam pulse can be accomplished by switching in a second set of fuses and switches (not shown in Fig. 2), which are similar to the set used in generating the first pulse. The 3-cm dia. cathode is constructed of saw blades. The anode plate is drilled with 0.5-cm dia. holes over an 8-cm dia. with a geometrical ratio of open area to total area of 0.68. At the typical charging voltages on C_o (240 µF) of $\simeq$ 9 kV and with $L_o \simeq$ 7 µH, pulses of $\simeq$ 180 kV with $\simeq$ 200 ns FWHM are produced. The beam current densities can be varied from 0.2 to 5 A/cm^2 by varying the anode-cathode separation. Because the e-beam pulse is so short, the discharge does not always have time to come to equilibrium. However, as long as the time histories of the beam current and voltage are known, investigations into how the basic physics of these discharges relate to EBCS applications and comparison to theory and numerical simulations can be carried out, as will be discussed in later sections.
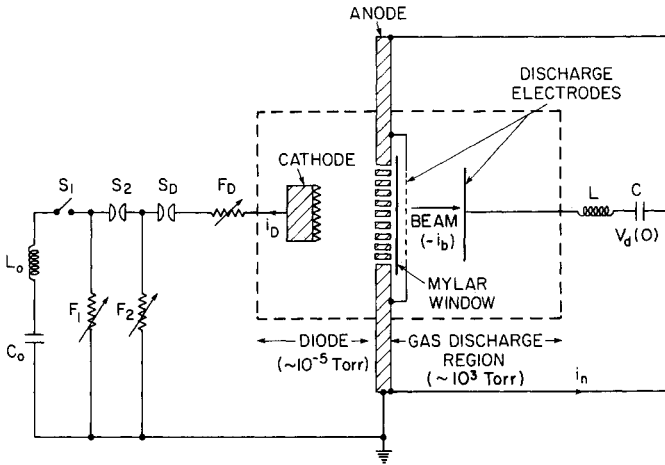

Fig. 2. Schematic of experimental apparatus.

Also schematically illustrated in Fig. 2 are the driving circuit and electrode structure for the gas discharge region. The current source driving the discharge in these experiments was a capacitor, C(1 µF), whose initial charging voltage $V_d(0)$ could be varied from 0-30 KV. The system inductance was measured to be L $\simeq$ 430 nH. The discharge electrode separation was 1 cm for all work discussed here. A copper screen of $\simeq$ 60% measured current transmission was used as the ground electrode. The 50-µm mylar window maintained a pressure differential between the discharge vessel and the evacuated ($\sim 10^{-4}$ torr) e-beam diode region while allowing the high energy portion of the e-beam to enter the discharge chamber. The apparatus has been operated at pressures of 1-7 atm. A Rogowski loop, located between the screen electrode and mylar window, was used to measure i_b, the e-beam current flowing into the discharge region. Additional diagnostics for this experiment include a voltage divider to measure the voltage across the diode, V_D; Rogowski loops to measure the diode current, i_D; and a commercial current monitor located at the driving capacitor to measure the net current in the discharge circuit, i_n. Shown in Fig. 3 are representative time histories of V_D, i_D, i_b and i_p.

where i_p is the discharge plasma current, for a 20% O_2 - 80% N_2 mixture with a ratio of applied electric field to gas pressure of 10.5 V/cm-torr. Because the polarity of the discharge was such as to accelerate plasma and e-beam electrons in the same direction, i_p is related to i_n and i_b by

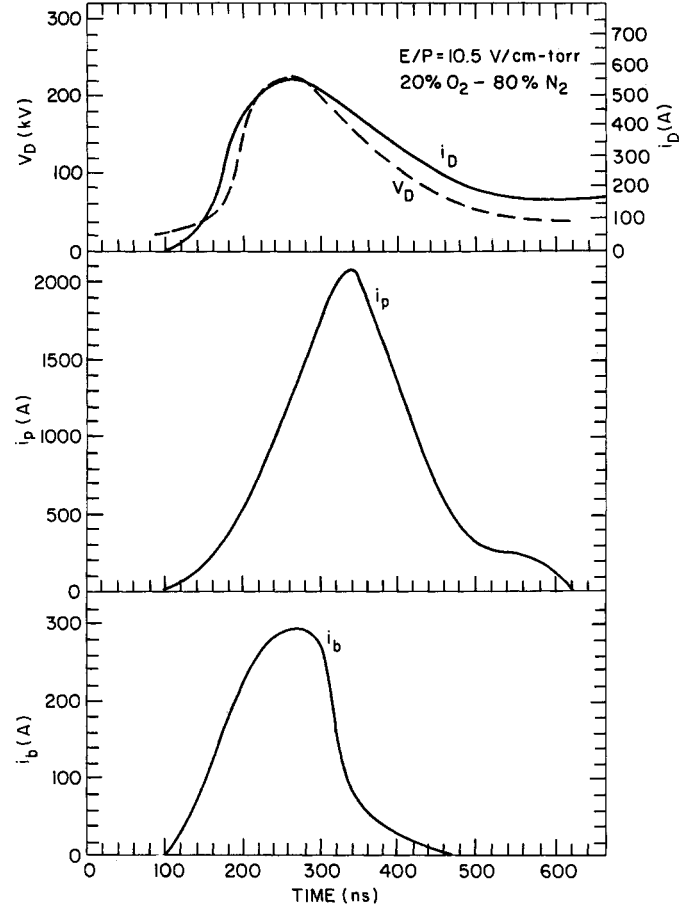$$i_p = i_n - i_b \quad . \tag{1}$$

Fig. 3. Representative time histories of discharge parameters obtained from standard diagnostics.

The circuit equation for the discharge is

$$V_d(0) = R(i_n - i_b) + L\frac{di_n}{dt} + \frac{1}{C}\int_0^t i_n dt, \tag{2}$$

where R is the discharge resistance. The discharge resistivity, ρ, is related to R through the discharge geometry only. Neglecting the last term in Eq. (2) (< 5-percent correction) we have at the time of peak i_n a discharge resistivity of

$$\rho_c = \frac{V_d(0)}{(i_n - i_b)} \quad \left(\frac{A}{\ell}\right) , \tag{3}$$

where A is the discharge area and ℓ the discharge electrode separation.

88

The resistivity of the discharge during conduction is one important characteristic. Another important parameter is the current gain, ε, defined as

$$\varepsilon \equiv \frac{i_n - i_b}{i_b^0} = \frac{i_p^0}{i_b^0} \quad . \tag{4}$$

where i_p^0 and i_b^0 are the peak values of i_p and i_b respectively. For a high energy transfer efficiency, $\varepsilon \gg 1$. The current gain for the data in Fig. 3 is $\simeq 7$.

Theoretical Model

Various aspects of the theoretical concepts associated with controlled diffuse discharges as they relate to the EBCS have been discussed.[4-7] In this section we give a cursory review of the physical model for the discharge. We describe a system in which a volumetric ionization souce produces a very weakly ionized gas. Typically, $n_p \sim 10^{-5} N_0$, where n_p is the plasma electron density associated with the ionizing e-beam and N_0 is the initial gas density. We assume electrode effects are not important, which is the case for applied voltages much greater than the sheath potential (< 1 kV).[6] Under these conditions the gas resistivity is determined by electron-neutral collisions, and the discharge potential is a linear function of the distance from the discharge electrodes.

We assume a two component gas mixture made up of a non-attaching base gas with some fraction of attaching gas. Because an attachment dominated recovery is desirable for EBCS applications,[4,7,8] we will ignore recombination. Assuming further that density gradients are negligible, the continuity equation for n_p gives

$$\frac{dn_p}{dt} \simeq S_0 J_b P - \alpha N_a n_p \quad . \tag{5}$$

Here S_0 is a beam ionization parameter,[8] $J_b (\equiv i_b/A)$ is the e-beam current density, α is the effective attachment rate coefficient(cm^3-s^{-1}), P is the total gas pressure and N_a is the density of the attaching gas. The first term on the right hand side of Eq. (5) represents the source of discharge plasma electrons. The mechanism for discharge plasma electron loss is represented by the second term on the right hand side of Eq. (5).

The discharge plasma density is related to the discharge plasma current density through

$$J_p \equiv i_p/A = n_p e v \quad , \tag{6}$$

where v is the electron drift speed,

$$v = \mu E \quad . \tag{7}$$

Here μ is the electron mobility[10] and E is the electric field across the discharge. Thus the discharge resistivity during conduction is given by

$$\rho_C = \frac{E_C}{J_p} = (e n_p \mu)^{-1} \quad , \tag{8}$$

where E_C is the electric field across the discharge during conduction.

We simulate the experiment by numerically solving a coupled set of rate equations, one for each ionic species, along with Eqs. (2) and (5). In this way n_p can be self-consistently obtained as a function of time for a given J_b and beam energy. It in turn may be used with Eq. (2) in Eqs. (6) and (8) to predict macroscopic observables in the experiment. An air-chemistry code, CHMAIR,[11] is used in solving Eq. (5). This allows many more atomic and molecular processes than those outlined here to be included. Comparisons between measured and calculated parameters will be discussed in the next section.

We replace the last term in Eq. (5) with a phenomenological expression, n_p/τ_p, where τ_p is the characteristic loss time for the discharge plasma electrons in the absence of ionization. Substituting n_p from Eq. (8) into Eq. (5), and noting that in equilibrium $dn_p/dt = 0$, Eq. (5) becomes

$$\frac{\varepsilon}{\tau_p} = (\frac{E_C}{P}) f_0 P \quad , \tag{9}$$

where $f_0 \equiv e S_0 \mu P$ is essentially a constant for a given gas composition. For most gases $f_0 \sim 10^5$ - 10^6 cm/V-s. Also, E_C/P will be approximately independent of pressure (see Sect. V). This analytic equilibrium scaling law has particular relevance for fast EBCS applications. In these applications one desires ε to be large and τ_p to be short. For a given gas composition, Eq. (9) indicates there is a "trade-off" between high ε and small τ_p while suggesting that operation at high pressure and mobility is favorable.

Overview of E-Beam Controlled Discharge Results

In this section we review several aspects of the experimental results and theoretical analyses that are particularly relevant to the design of an EBCS.

Figure 4 shows a comparison of the measured and predicted net discharge current i_n as a function of time at pressures of 1 and 3 atm for a 20% O_2 - 80% N_2 mixture. The code uses the measured i_b and diode voltage, V_D, to predict the circuit behavior. The measured e-beam current was modified so that only those beam electrons with sufficient energy to traverse the switch were used in the calculations. Because the code is zero-dimensional, it can not accurately predict what happens when beam electrons do not traverse the entire switch length as a result of either insufficient initial directed energy or excess transverse energy. This effect is particularly evident in the 3 atm case. To improve this comparison the e-beam electron energy must be increased. In making this comparison the screen electrode transmission of 60% and the time response of the Rogowski loop measuring i_b were taken into account. The code result was also

89

shifted 5-10 ns in time. The uncertainties in the code and measurement are estimated to be $\simeq$ 15% each. As can be seen from Fig. 4, the code accurately tracks the measured net current to within these uncertainties and the limits of the model. By using the results presented in Fig. 4, the scaling relation Eq. (9) can be checked. The values of τ_p obtained from the code are $\simeq$ 50 ns and $\simeq$ 20 ns for 1 and 3 atm respectively. Thus the ratio of (ε/τ_p) at 3 atm to (ε/τ_p) at 1 atm is $\simeq$ 4, compared to 3 from Eq. (9). The difference can be ascribed to the lack of equilibrium in the 1 atm. case.
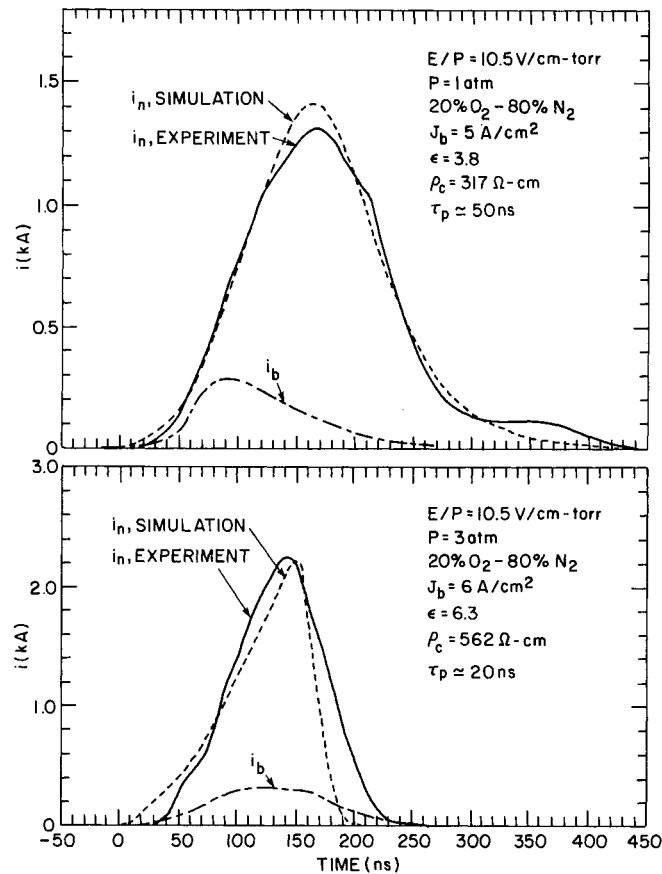

Fig. 4.   Comparison of measured and calculated net discharge current for 1 and 3 atm.

The switch performance can be optimized by choosing a gas or gas combination that exhibits a mobility and attachment rate which strongly vary with the time dependent electric field across the switch.[4,7,8,12] An example of such optimization is illustrated in Fig. 5 where ρ_c for a 10% O_2 - 90% N_2 and 10% O_2 - 90% Ar mixture is plotted for 1 atm as a function of initial applied voltage across the discharge, V_d (0) . This is also the voltage across the discharge when ρ_c is evaluated (Eq. (3)). In an actual application we desire ρ_c to be low during conduction, i.e., when V_d is low and increase during opening, when V_d becomes larger. We see that the Ar-O_2 mixture shows markedly different behavior from the N_2-O_2 mixture at different applied voltages. At low voltages (V_d(o)>1kV, for V_d(0) < 1 kV sheath effects dominate) the resistivity is 2 to 3 times lower for Ar-O_2 than N_2-O_2. As the voltage increases,

the opposite effect occurs with the resistivity for Ar-O_2 about 5 times higher than that for N_2-O_2.

A thorough analysis of this observation requires knowledge of the electron energy distribution, which we do not have at present. We
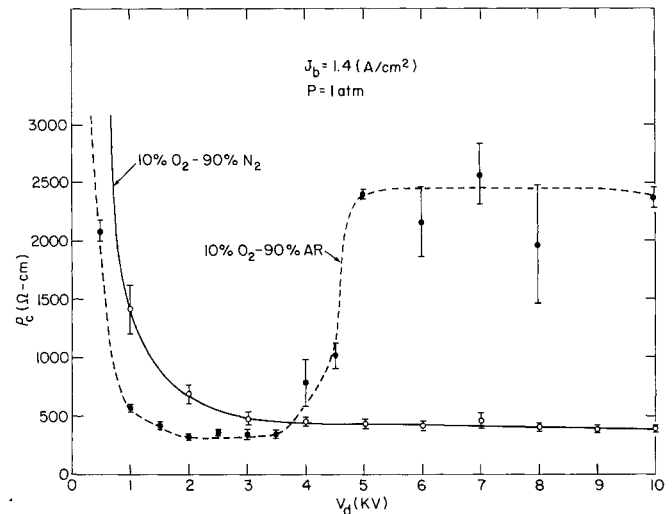

Fig. 5.   Comparison of discharge resistivity, ρ_c, for Ar-O_2 and N_2-O_2 mixtures as a function of initial voltage across discharge at 1 atm.

estimate[13] for the Ar case that the electrons have a mean energy ranging from 1-5 eV for the applied voltages in Fig. 5. This energy will be considerably lower in the N_2 case because of the accessibility of vibrational levels in N_2. At the pressure indicated (1 atm), two body dissociative attachment will dominate three body attachment for electron energies of ~ 5 eV. Also the Ramsaurer-Townsend[14] cross section for Ar is rapidly varying for electron energies between 0.5-5 eV. Thus the observed effect must be related to the higher mean electron energies in the Ar case, resulting in rapidly varying cross sections for momentum transfer and attachment. Control of the electron energy distribution function is therefore desirable in switch applications, as has been emphasized by Christophorou and co-workers.[14]

Discharge stability is of concern in either the repetitive or single pulse mode. The discharge stability can be affected by several processes. Changes in electrical and chemical properties of the switch gas[7] can result from heating of the gas, or as a cummulative result of the length of the conduction period or duty cycle. It may be possible to avoid some of these potential problems with the proper gas mixture.[15] Any reduction of E/N, where N is the gas density, either local or global at any time can trigger avalanche ionization. For example, an attachment instability[16-18] has been suggested as a cause of local increase in ρ_c , which when accompanied by local heating and a consequent decrease in N during the conduction phase of an e-beam substained discharge can result in a breakdown. Decreases in N resulting from heating at inhomogenities in the discharge or at electrodes has also been observed to cause breakdown.[18,19]

Under certain conditions in our experiment a breakdown is observed sometime after the e-beam

controlled discharge plasma current has stopped flowing. This effect is illustrated in Fig. 6, where the time to breakdown, τ_B, (measured from the initiation of i_p), is plotted as function of the peak discharge plasma current, i_p^0. This data was taken with a 10%-90% N_2 mixture at 1 atm. In order to observe this effect, the applied voltage must be 80-90% of the self break voltage. As seen in the figure, τ_B increases rapidly as i_p^0 (and the energy dissipated in the gas) is decreased. The measured times are of the order of acoustic transit times. This effect is not observed if the applied voltage is ⩽ 75% of the breakdown voltage, and is being studied further at present.
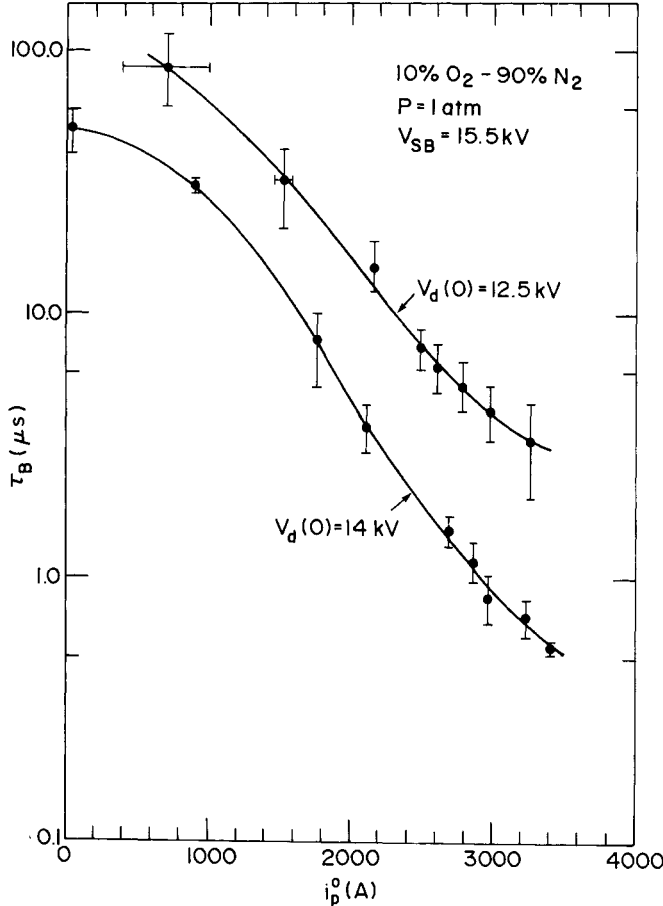

Fig. 6. Plot of time to breakdown, measured from the initiation of e-beam controlled discharge plasma current, as a function of peak e-beam controlled discharge plasma current, i_p^0.

Switch Design Formalism

The design of any EBCS must address two major concerns: (1) a required overall system efficiency must be satisfied; and (2) the self-sparking threshold must never be exceeded, so the switch gas can recover to its original dielectric strength. In this section we review a self-consistent procedure that can be used to estimate the switch gas composition, pressure, area, length, and e-beam generator characteristics for a given application. For details of this work, the reader should consult Ref. 8. This design formalism emphasizes the overall energy transfer efficiency of the switch-inductive store system, the circuit requirements, and the switch

physics. In what follows we assume the load pulse characteristics (current, voltage, FWHM) are specified a priori.

We begin by defining the energy transfer efficiency, η, as

$$\eta = \frac{n\, I_L^0 V_L^0 \tau_L}{(1/2)LI_{SW}^{0\,2} + nI_b V_b \tau_C} \qquad (10)$$

Here n is the number of pulses, I_L^0 and V_L^0 are the (single pulse) peak current and voltage delivered to the load, I_b and V_b are the (single pulse) e-beam current and voltage, L is the storage inductance, I_{SW}^0 is the peak switch current, τ_L is the characteristic load pulse width, and τ_C is the time interval during which the switch is conducting.

To elucidate better the energy loss terms, we rewrite Eq. (10) as $\eta = \xi/(\xi +1)$, where ξ, the gain factor, is the ratio of the energy delivered to the load to the total energy used in making the switch conduct. Thus

$$\xi = \frac{I_L^0\, V_L^0\, \tau_L}{[k_0 I_L^0 V_L^0 \tau_0 + I_{SW}^2 R_{SW}\tau_C + I_b V_b \tau_C]} \qquad (11)$$

where R_{SW} is the average switch resistance during conduction, I_{SW} is the average switch current during conduction, and τ_0 is the time interval during which the switch changes from conducting to nonconducting. The factor k_0 is a dimensionless constant that when multiplied by the peak power delivered to the load gives the average power dissipated in the switch during the opening phase. For resistive or inductive loads $k_0 \approx 0.25$.[8]

For reasonable energy efficiency ($\eta ⩾ 0.5$) we require $\xi ⩾ 1$. Therefore, each term in the denominator of Eq. (11) must be sufficienty less than the numerator. Thus we set

$$k_0\, I_L^0\, V_L^0\, \tau_0 = g_0\, I_L^0\, V_L^0\, \tau_L \quad , \qquad (12a)$$

$$I_{SW}^2\, R_{SW}\tau_C = g_C\, I_L^0\, V_L^0\, \tau_L \quad , \qquad (12b)$$

$$I_b\, V_b\, \tau_C = g_b\, I_L^0\, V_L^0\, \tau_L \quad , \qquad (12c)$$

where g_0, g_C, $g_b < 1$, such that

$$\xi^{-1} = g_0 + g_C + g_b < 1 \quad . \qquad (13)$$

The gas breakdown problem is avoided initially by satisfying the constraint

$$V_L^0 = s_B \frac{E_B}{P_0}\, (P\ell) \quad . \qquad (14)$$

Here V_L^0 is the maximum expected voltage across the switch (i.e., the peak load voltage), E_B is the static breakdown electric field at atmospheric pressure P_0, $s_B < 1$ is a dimensionless safety factor, and P is the switch pressure. Additionally, cummulative heating of the gas must be sufficiently constrained so that any reduction

in switch gas density does not significantly lower the self-sparking threshold. Energy is deposited in the switch primarily by resistive heating during the conduction phase, by resistive heating during the opening phase, and by direct deposition by the e-beam. Thus, a second constraint to avoid breakdown is a

$$n \left[k_0 I_L^O V_L^O \tau_0 + I_{SW}^2 R_{SW} \tau_C + k_b I_b V_b \tau_C \right] =$$
$$s_H \left(\frac{W_B}{P_0} \right) A(P\ell) \qquad (15)$$

Here k_b is the fraction of the beam energy deposited in the switch gas, s_H is a dimensionless safety factor, and W_B is the deposited energy per unit volume required for breakdown at atmospheric pressure.

We may now proceed to compute the switch pressure. Using Eqs. (12a,b,c) and (14), the definition of ϵ, scaling relation Eq. (9), and recalling that $E_c = I_{SW} R_{SW}/\ell$ we have

$$P^{-1} \simeq \frac{g_0 g_c g_b s_B f_0}{k_0 k_p} \tau_L \frac{E_B}{P_0} \left(\frac{V_L^O}{V_b} \right) \left(\frac{\tau_L}{\tau_C} \right)^2 \qquad (16)$$

The factor $k_p \equiv \tau_0/\tau_p$ is the number of τ_p periods necessary for the switch to interrupt the current when the beam current is zero. Using Eq. (5) with the ionization term set to zero, one can show that $k_p \sim 5$ for an attachment dominated switch.[7,8] The fraction of attaching gas can be estimated from the calculated pressure, required efficiency, and known attachment rates. The "g" factors in Eq. (16) are chosen so that P can be small (for ease of switch construction) consistent with the constraint of Eq. (13). An optimum choice for g_0, g_c, and g_b can be obtained by using the method of Lagrange undetermined multipliers. This removes the implied arbitrary nature of Eq. (13). The result is $g_0 \approx g_c \approx g_b$. For example if η is chosen to be 0.75, then $\xi=3$ and $g\approx0.1$.

Once P is known, Eq. (14) gives the switch length, ℓ, and Eq. (15) gives the switch area, A. The switch dimensions thus computed insures that the switch will be large enough that the breakdown threshold will not be reached.

The e-beam generator requirements are determined from V_b, I_b, and A. I_b is computed from Eq. (12c). The e-beam generator must actually provide a somewhat higher current than I_b to account for current lost to the structure supporting the interface between vacuum and high pressure. The e-beam generator must also supply a beam of area A. Note that in order for the beam to traverse the switch length V_b will depend on the product $P\ell$, as does V_L. Therefore, one can show that typically $V_b \simeq V_L$, with $k_b \simeq 0.3$.

Single Pulse System

In this section we outline the design of a single pulse, high power ($\sim 6 \times 10^9$ W), inductive storage system presently under construction. The circuit requirements are presented first. The design procedure outlined in the previous section is then used to determine the switch parameters.

Figure 7 is a circuit diagram of the proposed system. The desired load pulse parameters are

peak load current of $I_L^O \simeq 30$ kA, peak load voltage of $V_L^O \simeq 200$ kV, and load pulse width of $\tau_L \simeq 100$ ns. This choice of parameters is relevant to several pulse power applications.[3,8] For technological reasons dealing with the beam decay time, we take $\tau_0 \simeq 100$ ns. We chose the storage inductance charging time to be $\tau_C \simeq 10 \tau_L$ or 1 μs. Thus the quarter period of the charging circuit (the switch conduction time) is 1 μs, giving for a (typical) 1 μF capacitor, a system inductance of $L \simeq 0.65$ μH. I_{SW}, the peak value of the switch current, is $\approx I_L^O$. This gives a charging voltage for the capacitor of $V_{SW}^O \simeq 25$ kV. The voltage produced is then $V_L \simeq L(I_L^O/\tau_0) \simeq 200$ kV.
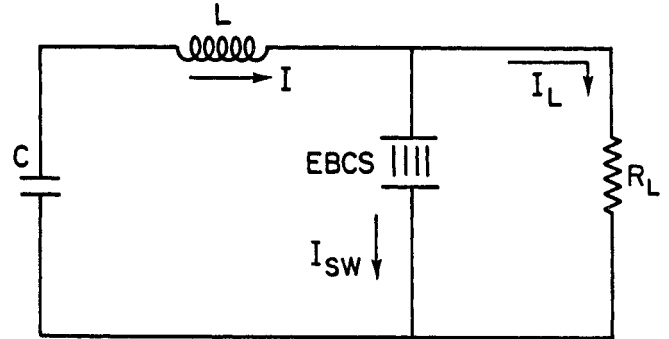

Fig. 7. Schematic of single pulse, inductive storage generator using an EBCS.

We choose an energy transfer efficiency of $\eta = 0.5$, assume the switch will be attachment dominated giving $k_p \simeq 6$, take $k_0 = 0.25$ for a resistive load, $s_B = 0.75$, $s_H = 0.5$, $E_B = 20$ kV/cm, and $W_B = 0.15$ J/cm^3.[8] Then the results of the previous section can be used to obtain the following parameters: $P \simeq 12$ atm (Eq. (16)), $\ell \simeq 1$ cm (Eq. (14)), and $A \simeq 350$ cm^2, radius $\simeq 10$ cm (Eq. (15)). The current gain, from Eq. (12C) with $g_b \simeq 0.3$, is $\epsilon \simeq 30$. This gives an e-beam current of $I_b \simeq 1$ kA. The beam decay time should be $<< \tau_0$.

Conclusion

The results of this work indicate that the EBCS is a viable opening switch concept. Experiments with e-beam controlled discharges verify the conceptual understanding of the physics which govern the switch behavior. Discharge parameters may be optimized for switch application through proper choice of gas mixture and operating regime. Backed by this understanding an EBCS design procedure was outlined and a single pulse system was designed to demonstrate a high power ($\sim 6 \times 10^9$ W) inductive store - opening switch system.

References

1. R.D. Ford, D. Jenkins, W.H. Lupton, and I.M. Vitkovitsky, Rev. Sci. Inst. 52, 694 (1981).
2. S.A. Nasar and H.H. Woodson, Proceedings of the Sixth Symposium on Engineering Problems of Fusion Research, IEEE Pub. No. 75CH1097-5-NPS (1975), p. 316.
3. W.A. Barletta, Lawrence Livermore Laboratory Report UCRL-87288 (1981).
4. R.J. Commisso, R.F. Fernsler, V.E. Scherrer, and I.M. Vitkovitsky, IEEE Trans. Plasma Sci. PS-10, 241 (1982) and references therein.
5. L.E. Kline, ibid, p 224.
6. M.R. Hallada, P. Bletzinger, and W.F. Bailey, ibid, p. 218.
7. R.F. Fernsler, D. Conte, and I.M. Vitkovitsky, IEEE Trans. Plasma Sci. PS-8, 176, (1980).
8. R.J. Commisso, R.F. Fernsler, V.E. Scherrer, and I.M. Vitkovitsky, Naval Research Laboratory Memo Report 4975 (1982). To be submitted to Rev. Sci. Inst.
9. B. Fell, R.J. Commisso, V.E. Scherrer, and I.M. Vitkovitsky, J. Appl. Phys. 53, 2818 (1982).
10. S.C. Brown, Basic Data of Plasma Physics (MIT Press, Cambridge, 1967), pp. 87-94.
11. R.F. Fernsler, A.W. Ali, J.R. Grieg, and I.M. Vitkovitsky, Naval Research Laboratory Memo Report 4110 (1979).
12. L.G. Christophorou, S.R. Hunter, J.G. Carter and L.A. Mathis, Appl. Phys. Lett. 41, 147 (1982).
13. J.W. Dzimianski and L.E. Kline, Final Technical Report No. 80-0120, Aero Propulsion Laboratory, Wright-Patterson AFB (1979).
14. J.B. Hasted, Physics of Atomic Collisions (American Elsevier, New York, 1972), pp. 306-310.
15. L. Christophorou, paper in this conference.
16. D.H. Douglas-Hamilton and Siva A. Mani, Appl. Phys. Letter. 23, 503 (1973).
17. D.H. Douglas-Hamilton and S.A. Mani, J.Appl. Phys. 45, 4406 (1974).
18. M.N. Andreeva, I.G. Persiantsev, V.D. Pis'mennyi, V.M. Polushkin, A.T. Rakhimov, M.A. Timofeev, and E.G. Treneva, Sov. J. Plasma Phys. 3 (6), 770 (1977).
19. S.A. Genkin, Yu. D. Korolev, V.G. Rabotkin, and A.P. Khuzeev, Sov. J. Plasma Phys. 7 (3), 327 (1981).